AIP | Review of Scientific Instruments

Discharge tube with coaxial geometry for efficient production of metal hydrides

I. Bozhinova, St. Kolev, M. Dimitrova, Tsv. Popov, and A. Pashov

Citation: Rev. Sci. Instrum. **84**, 093107 (2013); doi: 10.1063/1.4820959
View online: http://dx.doi.org/10.1063/1.4820959
View Table of Contents: http://rsi.aip.org/resource/1/RSINAK/v84/i9
Published by the AIP Publishing LLC.

Additional information on Rev. Sci. Instrum.

Journal Homepage: http://rsi.aip.org
Journal Information: http://rsi.aip.org/about/about_the_journal
Top downloads: http://rsi.aip.org/features/most_downloaded
Information for Authors: http://rsi.aip.org/authors

ADVERTISEMENT

Discharge tube with coaxial geometry for efficient production of metal hydrides

I. Bozhinova,[1,2] St. Kolev,[1] M. Dimitrova,[2] Tsv. Popov,[1] and A. Pashov[1]
[1]*Department of Physics, Sofia University, 5 James Bourchier Boulevard, 1164 Sofia, Bulgaria*
[2]*Emil Djakov Institute of Electronics, Bulgarian Academy of Sciences, 72 Tsarigradsko Chaussee, 1784 Sofia, Bulgaria*

(Received 13 June 2013; accepted 26 August 2013; published online 30 September 2013)

The production of metal hydrides in vapour phase is one of the problems which makes their spectroscopic investigation at high resolution difficult. The molecular densities are usually low and the absorption is often increased by the use of multipass cells or intracavity setups. In this contribution a discharge tube with coaxial geometry is investigated, which is able to produce relatively high densities of NiH ($\approx 10^{12}$ cm^{-3}). Additional advantage of the present geometry is that the densities are very homogeneous along the discharge length, 250 mm in our case, which can be made in principle arbitrary long. As a result, reliable absorption was detected even in a single pass experiment. We also present the results of a numerical model which explains the general properties of the plasma in the tube. Based on this understanding, we discuss possible improvements and other applications of this discharge geometry. © *2013 AIP Publishing LLC*. [http://dx.doi.org/10.1063/1.4820959]

I. INTRODUCTION

Gas discharge tubes are often employed as sources of molecules and radicals.[1–3] These species usually have short lifetimes or their vapour pressure at reasonably high temperatures is very low. The discharge introduces a spectroscopic medium affected by collisions and the background radiation of the collisionally excited gas. Effects of the various types of collisions are of less significance in experiments, where Doppler limited resolution is sufficient. The background radiation is acceptable in absorption experiments, however, it disturbs the emission experiments and mainly the Fourier transform spectroscopy of Laser Induced Fluorescence (LIF), where the noise level in the spectra depends on the overall intensity of the light on the detector. One of the big challenges in the design of a discharge tube is to achieve a homogeneous column of molecules with lengths and densities sufficient to ensure detectable absorption coefficients.

In Refs. 4 and 5, a new design of discharge tube was introduced. It consists of a sectional cylindrical cathode which surrounds the anode made of metal mesh in the form of a tube. The length of the two electrodes was about 500 mm, but the sectional construction of the cathode allows a discharge tube with arbitrary length and homogenous discharge to be built. References 4 and 5 were devoted to probe measurements in argon and oxygen plasma. The authors have observed that at a specific range of gas pressures and currents the discharge in argon is concentrated mainly between the two cylindrical electrodes and the volume inside the anode surface is dark. These observations motivated us to investigate in detail this configuration of electrodes and its possible application for production of molecules and in spectroscopy because we expected here several advantages over the traditional hollow cathode sources. First of all, it is the large absorption path (due to the length of the electrodes). This would be of advantage both in absorption and in LIF setups. Second, it is the large volume free from background radiation—important for Fourier transform spectroscopy. Then, because of the large cathode area and the specific geometry of the tube we expect much lower heating and sputtering of the cathodes at comparable concentrations of metal hydrides. Here, it should be stressed that the present geometry should not be considered as an alternative to the widely used hollow cathode discharges. Depending on the particular application, the researcher should choose the most suitable source and this is one of the motivations to characterize coaxial geometry.

In order to test the possible applications of the coaxial discharge tube in spectroscopy we decided to run in parallel a numerical simulation and an experiment. The simulation should be able to model the discharge in the given geometry. We are particularly interested to be able to predict the conditions (gas pressure and current) at which a dark central zone is formed. This is expected to depend mainly on the type of the gas and the geometry of the tube and to a much less extent on the material of the cathode. Another task, also very important, is to assess the density distribution of the produced molecules. It is much more complicated and needs information about the reactions forming molecules and their rate coefficients for every type of cathode material which is not always available. Therefore, within this contribution we decided to concentrate our efforts on the first task only.

Within the experiment it was important to construct a discharge tube better suited for spectroscopy than the original design[4,5] (see the explanations below). We planned to make the first cathodes from Ni and to investigate the performance of the tube together with the production of NiH molecule. This was motivated by the existence of several different discharge sources for NiH, so that a reliable comparison could be made. Absorption spectra of NiH are well studied in the green and the red spectral regions.[3,6] Therefore, it should be possible to assess the production of molecules by the absorption of known spectral lines.

 © 2013 AIP Publishing LLC

The paper is organized as follows: In Sec. II, detailed notes on the construction of a prototype of the discharge tube are provided. The experimental test of the prototype is reported in Sec. III. Here the performance of the tube is compared with existing sources from the literature. In Sec. IV the numerical model of the discharge tube is presented. In Sec. V we analyze the results and compare the numerical calculations with the experimental observations. Finally, in Sec. VI we discuss the future development of this source.

II. CONSTRUCTION OF THE DISCHARGE TUBE

For testing of the coaxial geometry of the discharge tube initially we assembled a prototype which is very close to the original tube from Refs. 4 and 5. In the original construction, the anode was made of a fine mesh from stainless steel (see Fig. 1). Since we expected that it will prevent the diffusion of molecules from the discharge area to the center of the tube, it was decided to replace the mesh with a set of six metal rods (stainless steel, diameter 1 mm) lying axially on the cylindrical surface (with a diameter of 30 mm), formed previously by the mesh. The diameter of the eight Ni cathode rings is 66 mm and the width of each of them is 26 mm. They are placed at a distance of about 6 mm (edge to edge), forming a total length of about 250 mm. The anodes are somewhat longer (about 300 mm). The electrodes are placed in the central part of a glass tube (74 mm outer diameter and 470 mm in length). For applying the cathode voltage, separate feedthroughs with electrical connection are built for each of the cathodes. All the anode rods are connected electrically together by the metal supporting rings and one additional feedthrough is attached to the glass tube for this electrode. Both ends of the glass tube are cut at a small angle (about 10°) and closed with aluminum flanges which carry the tube windows (40 mm diameter). Two vacuum connections are also attached to the discharge tube. They are made of glass tubes with KF16 flanges made of aluminum and fixed to the glass with epoxy.

The cathode rings were rolled from 0.2 mm thin Ni foil and fixed by point welding. Additionally, a M3 nut is welded to each ring at the point where the electrical connection is attached. The feedthrough consists of a small tube (with a diameter of 10 mm) welded to the main tube and a cup with the same diameter and a prewelded tungsten wire (1 mm diameter). A M3 screw is attached to the wire for connection with the cathode. The assembling is done in the following way: First the cathode ring is inserted into the place, with the nut just beyond the glass tube of the feedthrough. Then the tube is closed with the cup while rotating it and fixing the screw into the nut. The length of the tungsten wire should be carefully estimated such that after fixing the screw the ends of the tube and the cup come into contact. Then the connection is sealed either by epoxy or silicone (hot gun). The silicone has worse vacuum properties, but the practice has shown that sealed in this way the tube leaks with a rate of about 0.18 Torr l/h, which turns out to be sufficient for experiments with gas flow or even short scans without flow. On the other hand, the silicone connections can be easily disassembled (for example, to replace the cathodes) and reassembled.

For the discharge a variable DC high voltage source ($U_{max} = 1$ kV, $I_{max} = 300$ mA) with grounded anode was used. For stable discharge each cathode was supplied through a separate 5.6 kΩ resistance. The total current (I_t) was controlled by varying the source voltage.

After closing the new tube it needed to be conditioned for several days by continuous pumping with rotational pump ($\sim 10^{-3}$ mTorr) under periodic running of the discharge at 200 mA current (for several tens of minutes) with Ar as a buffer gas. Once in a good condition (leaks less than 0.018 Torr l/h), even after being aired for short periods of time, the tube was ready for experiments after few hours of conditioning.

III. EXPERIMENTAL SETUP

To test the prototype of the discharge tube, the experimental setup for absorption spectroscopy shown in Fig. 2 was collected.

The laser source is a commercial free-running diode laser, scanned in frequency by the current and temperature (635 nm and 10 mW of optical power). Three beamsplitters (BS) guide the laser beam. The main beam passes through the discharge tube and its intensity is measured by the photodiode (PDx). The rest three beams are derived from it by splitting. The first one goes to the photodiode (PDy) for calibration of the laser power. The second and the third are used for

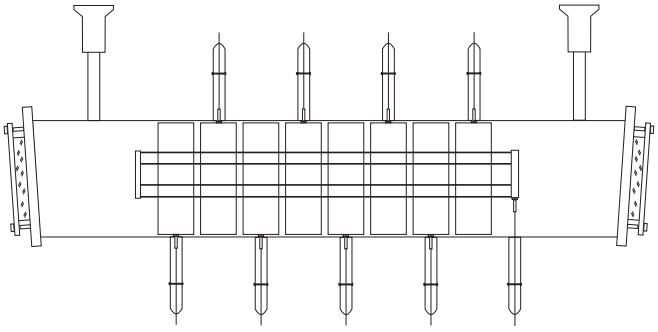

FIG. 1. Schematics of the prototype of the coaxial discharge tube, used in the present study. The electrodes are fixed in a glass tube equipped with feedthroughs for electrical connections and two windows for optical access.

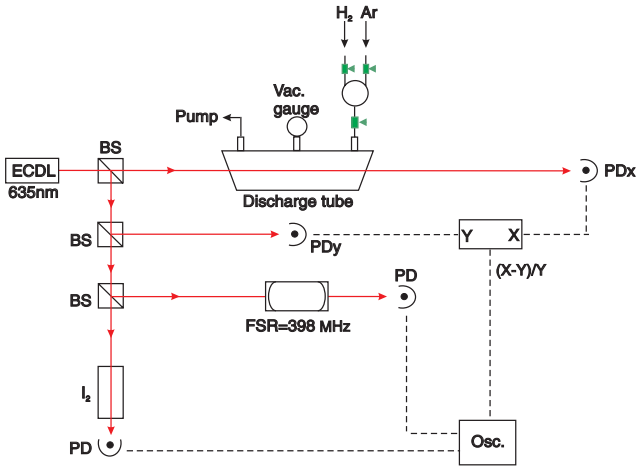

FIG. 2. The experimental setup for absorption spectroscopy.

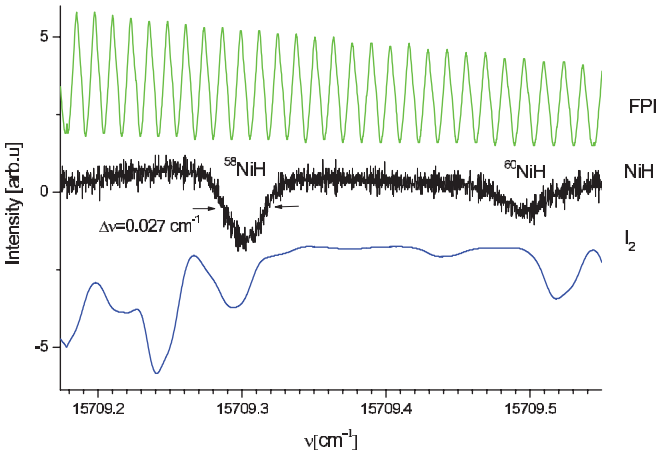

FIG. 3. A typical absorption spectrum that reveals the P(8.5d) line in ^{58}NiH and ^{60}NiH: Interference fringes (top signal in green), two NiH lines (middle signal in red), and iodine lines (bottom signal in blue).

calibration of the laser frequency by a confocal interferometer, with a free spectral range of 398 MHz and a 300 mm long iodine cell at room temperature. The signals are collected and recorded by a Tektronix TDS 2024 digital oscilloscope.

Initially, the experiments were performed with a gas mixture of 90% Ar and 10% H_2 because this proportion was reported to be optimal in Refs. 1 and 2. Unfortunately, in our case no signal was detected at these conditions. Weak absorption signal was detected only in pure hydrogen atmosphere. After adding small amounts of Ar in the discharge volume, the NiH density drops below our detection limit. In this sense the working conditions of our source are similar to those from Ref. 3 where measurements were carried out in a pure hydrogen atmosphere as well.

Within the range of single mode generation of the laser, several transitions of the red NiH band were chosen in order to examine the influence of the discharge parameters on the NiH concentration. Fig. 3 shows one of the obtained absorption spectra of NiH isotopomers belonging to ^{58}NiH and ^{60}NiH (the natural isotopic abundance of nickel is 68.1% (^{58}NiH) and 26.2% (^{60}NiH)[7]). The laser was scanned by ± 0.3 cm^{-1} around the P(8.5d) transition (15709.264 cm^{-1}).[3]

The obtained NiH signals are very weak. The trace shown in Fig. 2 is a result of 128 averages and corresponds to an absorption of about 0.02% for the main isotopomer ^{58}NiH. The Doppler width is estimated from the profile of the spectral line and its value is $\Delta\nu = 0.027$ cm^{-1} which corresponds to gas temperature of about $T = 340$ K.

Two additional absorption lines (P(8.5c) at 15706.409 cm^{-1} and P(6.5d) at 15804.030 cm^{-1})[3] were examined in a similar manner. In each case, a shift of the transition frequency between our calibration and the data from Ref. 3 was noticed as follows: 0.038 cm^{-1} for P(8.5d), 0.009 cm^{-1} for P(8.5c), and 0.013 cm^{-1} for P(6.5d).

A. Determination of NiH molecules concentration

The concentration of NiH molecules was monitored through their absorption in the (0,0) band of the $B^2\Delta_{5/2}$–$X^2\Delta_{5/2}$ transition. Having the experimental spectrum we can estimate the relative absorption coefficient in the center of the spectral line by the following relations:

$$\Delta I/I = \sigma(\nu_0) N_J L, \quad \text{where} \quad \sigma(\nu_0) = \frac{2\lambda^2 A_{00}}{8\pi\,\Delta\nu_D}\sqrt{\frac{\ln 2}{\pi}}. \tag{1}$$

From here we can obtain the population density of the NiH molecules for a particular ro-vibrational level N_J, provided the absorption cross-section of the transition P(8.5) is known. L is the absorption length, λ is the wavelength, and A_{00} is the Einstein coefficient for spontaneous emission, in our case, from the upper level ($v' = 0$, $J' = 7.5$) to the lower level ($v'' = 0$, $J'' = 8.5$) of the electronic transitions.

To obtain the value of A_{00} and subsequently to estimate σ and the total density of NiH molecules N_{tot}, we make two important assumptions. From Ref. 1 it is known that the lifetime of the ro-vibrational levels with $v' = 1$ of the $B^2\Delta_{5/2}$ state is about 1 μs. Looking at the spectra from Ref. 2 it becomes clear that the overall LIF after a laser excitation of $B^2\Delta_{5/2}$ ($v' = 1$) levels is about 20 times more intensive than the fluorescence after exciting $B^2\Delta_{5/2}$ ($v' = 0$). If we assume that the induced fluorescence is a measure of the number of the excited molecules, we can estimate the transition (X ($v'' = 0$) to B ($v' = 0$)) as 20 times weaker than the (X ($v'' = 0$) to B ($v' = 1$)) one and consequently $A_{00} \approx A_{01}/20$. The second assumption is a thermodynamic equilibrium (Boltzmann distribution) over all the ro-vibrational levels ($T = 340$ K).

Under these assumptions, we can estimate a maximum concentration of $N_J \approx 10^{11}$ cm^{-3} for $J = 8.5$ (corresponding to the 0.02% absorption) and $N_{\text{tot}} \approx 10^{12}$ cm^{-3} for the total density of molecules. Although very rough, this estimation shows a better performance of this source compared with other gas discharge sources, e.g., in Ref. 1 where the authors report a concentration of $N_{\text{tot}} \approx 10^{10}$ cm^{-3}.

The observed decrease of the NiH signal with the increase of the gas pressure can be understood as a consequence of the lower ion energy at the cathodes and the lower sputtering rate. The electron temperature also decreases with the increase of the pressure (due to more efficient ionization and lower diffusion losses). Therefore, we can argue that the decrease of the radiation in the center of the discharge is connected to the smaller energy of the electrons. In order to find the detailed balance between the NiH production and the emission of radiation, more quantitative description of the discharge is needed.

IV. NUMERICAL MODEL DESCRIPTION

The numerical model used here is an explicit Particle In Cell Monte Carlo Collision (PIC-MCC) simulation. The method used is based on the classical leap-frog algorithm scheme, given in Ref. 8. The PIC-MCC numerical technique provides the solution of the Boltzmann equation for the considered species, and thus it provides an accurate distribution function and resolves the full plasma dynamics. The major drawback of the explicit PIC-MCC method, compared with the fluid approach, is the considerable computational resources required for plasma, with high density in 2 and

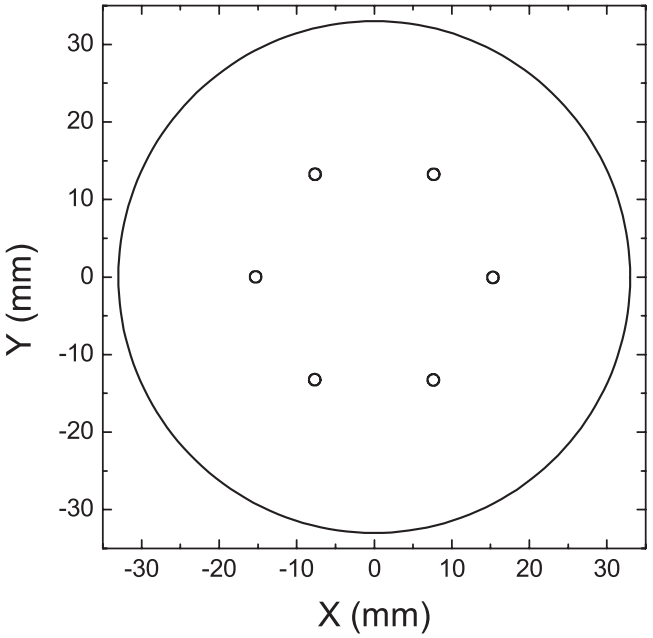

FIG. 4. Geometry considered in the model. Half of this ($x \geq 0$) is actually modeled.

3 spatial dimensions. We have "experimented" with fluid modeling of the discharge as well. However, it appears that the fluid model has troubles to resolve accurately the electron energy distribution function (EEDF) and also the collision dynamics. This is especially true for the central part of the discharge where accurate EEDF and averaged energy is important for the description of the collision processes, which we will use as an estimation for the light emitting properties of the discharge.

The species considered in the simulations are electrons, H, H_2, H^+, H_2^+, and H_3^+. The H_2 and H densities are considered as fixed and homogeneous along the domain. The H/H_2 ratio was calculated from a fluid model using H_2 dissociation rate determined from the PIC-MCC model. The obtained H density was much less than 5% due to the relatively fast conversion to H_2 on the walls. Thus, the H atoms will play a small role in the overall balance and therefore we fixed their density to 1% from the total neutrals density and used in the model for diagnostic reasons. The model is two dimensional both in the configuration and the velocity space. The geometry considered in the simulations is shown in Figure 4. The 2D simulation plane corresponds to a cross-section in the middle of the discharge tube (see Fig. 1), i.e., an infinite discharge in the axial direction is assumed due to the relatively large ratio between the discharge length and the diameter of the cathodes. Actually, in the numerical calculation the geometry is further reduced by taking advantage of the geometrical symmetry—we consider only half of the discharge cross section, including three anode rods. More detailed information about the model is presented in the Appendix.

An important parameter in the model is the secondary electron emission coefficient (k_{sec}). This parameter depends on the ion energy, ion (gas) type, cathode material, and in some cases it may depend also on the cathode surface properties. We were not able to find sufficient data for k_{sec} on the

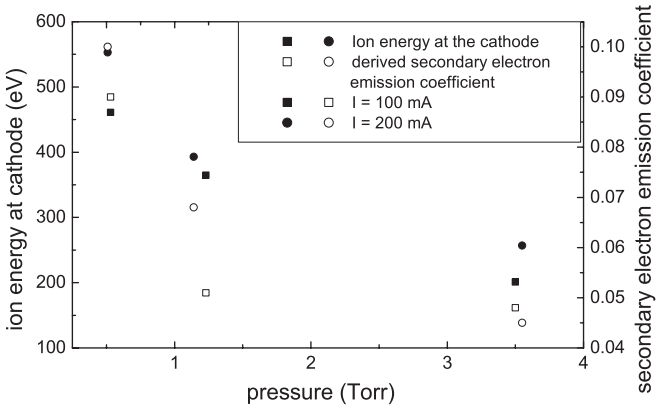

FIG. 5. Variation of the incident ion energy at the cathode surface and the obtained secondary electron emission coefficient as a function of the gas pressure. The total cathode current is noted in the figure.

Ni cathode in the case of H^+, H_2^+, and H_3^+ ions. However, even if managed to do that, it is not clear whether they correspond to the cathode surface in our device, because no special care is taken for the cathode surface cleaning in our experiment. Therefore, a kind of hybrid approach between the experiment and the numerical model was applied. During the experiments, the cathode-anode voltage drop and the cathode current were measured. Then the experimental value of the voltage drop was applied as a boundary condition for the Poisson equation and an effective k_{sec} (equal for all ion species) was fitted until the numerically calculated current matches the experimental one. Fig. 5 presents the obtained values for the effective secondary electron emission coefficient (right vertical axis). The coefficient is assumed to be equal for all ion species and, as it should be expected, it increases with the ion energy. We are not able to comment on the particular shape of the dependence—it is probably specific for different material surfaces and experiments. Additionally, numerical tests were carried out in order to study the model sensitivity to k_{sec}. It was found that if the current is fixed, the plasma density and the electron temperature are more or less the same for a wide range of k_{sec} variation (from $k_{sec}/2$ to $2k_{sec}$, where k_{sec} is the value obtained by adjusting the model boundary conditions to the experimental current/voltage data).

V. RESULTS AND DISCUSSION

A. The discharge tube as a source of NiH

In Figs. 6(a) and 6(b) the dependences of the absorption of the NiH species (at the same spectral line) on the main parameters (pressure and current) are shown. The pressure dependence (Fig. 6(a)) gives optimum conditions for maximum NiH density (200-300 mTorr) while the current dependence of the density (Fig. 6(b)) is very close to linear. We noticed that at the given current and gas pressure the absorption decreases with the temperature of the tube. Therefore, we did our best to keep a constant and low temperature of the tube when recording the current and pressure dependences. In order to check the consistency of the collected data and to get an impression about the experimental uncertainty, some

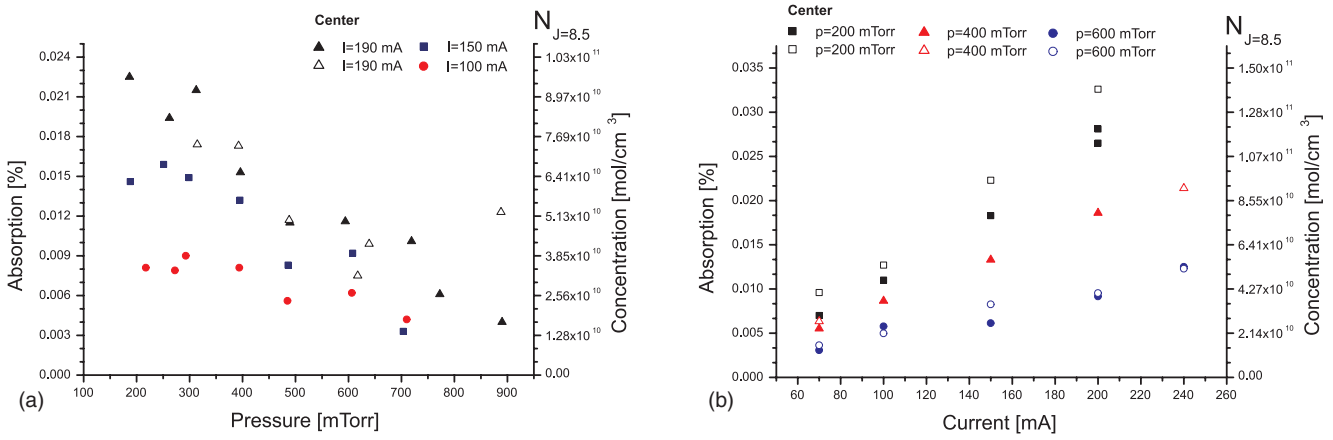

FIG. 6. Dependence of the relative absorption and (in the left vertical axis) the NiH density from (a) the pressure and (b) the current measured in the center of the tube.

measurements were repeated and are also shown in Fig. 6. We were able to vary the current only in the range from 70 mA to 240 mA. Further increase of the current was not possible due to the current power supply and the lack of cooling system in our plasma source.

We also examined the behaviour of the absorption signal with respect to the gas flow. Stronger signals were measured without gas flow, so all the measurements were done in this regime. To verify whether the distribution of the NiH species is homogeneous in the central region of the tube, we did measurements in the center of the tube and close to the anode. In both cases, the obtained/observed values of the relative absorption and respectively the density of NiH species were similar.

Since the tube was operated with no gas flow, it is worth mentioning our observations on the hydrogen adsorption and desorption on the cathode surface. After the end of a measurement, when warm tube was left under few hundreds of mTorr of gas pressure, we observed a significant drop of the pressure (several tens and even hundreds of mTorr) as the tube got colder. We explained this by the adsorption of hydrogen to the cathodes. Alternatively, when starting a new measurement (cold tube and cathodes) and filling the tube at the given pressure of hydrogen, after starting the discharge we observed a gradual increase of the gas pressure following the warming of the cathodes. We believe that there is a correlation between the desorption of hydrogen from the cathodes and the drop in the NiH signal. If we assume that nickel hydrides are formed on the cathodes following the reaction between the adsorbed hydrogen molecules and sputtered Ni atoms, it is possible to explain the drop in the NiH signal after heating the cathodes (similar behaviour was also observed in Ref. 2).

The optimal conditions for NiH production in this tube are at relatively low pressures, however, then the plasma fills and emits light from the entire volume of the tube including the central region. It was found that the desired dark region in the center of the tube occurs at higher pressure (above 2 Torr) and at lower current but in these cases we did not observe any absorption signal. Since we are interested in applications of this discharge geometry also for LIF experiments, when analyzing the results of the experiment and the numerical simulation, we tried to find the factors responsible for emission of the plasma in the visible range and NiH production.

B. General discharge behaviour

The discharge behaviour in general is related to the gas pressure and the deposited power (cathode current and voltage). An interesting feature of the present discharge is the existence of almost field-free region in the central part between the anodes, where the plasma exists due to diffusion and thermal conductivity. In the simulation the anodes are considered at potential 0 V and the cathode is negatively biased. Without plasma, the center region must be completely field-free. However, the accumulation and production of charged particles in the center changes that. In Fig. 7 a result of the PIC-MCC simulation is shown and one can see that a positive potential is established there, caused by the ambipolar field due to different diffusion speeds of the electrons and the positive ions to the walls (anodes). The accumulation of plasma in the initially field-free central region leads to establishment of a small positive potential (see Fig. 7) with respect to the anodes, which is determined by the electron temperature (T_e)—the higher the electron temperature the higher the potential.

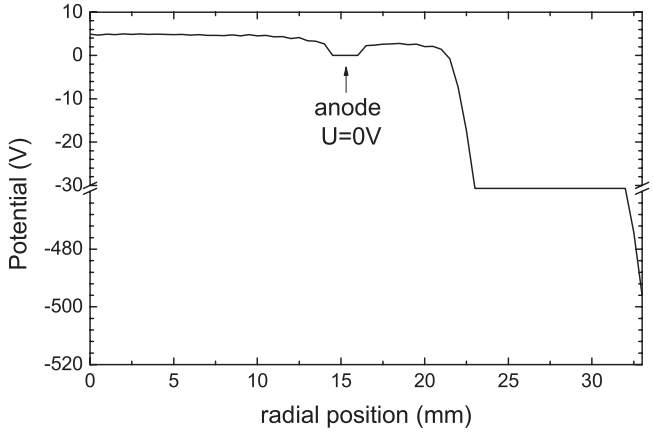

FIG. 7. Radial potential profile through the center of one anode: $p = 1.14$ Torr, $U = 496$ V, and $I = 200$ mA. An axis break is introduced for better visibility of the central region.

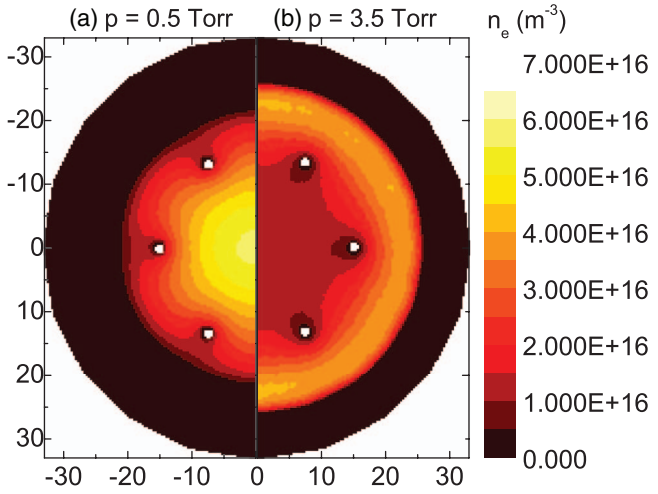

FIG. 8. Electron density distribution for two cases: (a) $p = 0.5$ Torr, $U = 590$ V and (b) $p = 3.5$ Torr, $U = 292$ V. Both cases are for total current $I_t = 200$ mA.

In Fig. 8 the electron density distribution obtained from PIC-MCC model is shown. From this figure and Fig. 7 one can see that at relatively high current and relatively high pressure the plasma extends towards the cathode, beyond the anodes. In this case the whole voltage drop (see Fig. 7) is concentrated between the plasma "column" and the cathode (not between the anode itself and the cathode). At low pressure, the plasma is limited in the central region only (Fig. 8(a)) and has a maximum density at the discharge center. At higher pressure, the charged particles produced between the anode and cathode diffuse slower to the central region. The slower diffusion combined with weaker energy transport and with recombination of charged particles even lead to lower density in the center compared to the anode-cathode region (Fig. 8(b)).

Apparently, the discharge behaviour is highly dependent on the gas pressure. The pressure increase normally leads to reduction of the particles mobility and to more efficient ionization—single electron experiences more collisions during its cathode-anode drift. With respect to spectroscopy applications (and particularly for LIF) of the source, a crucial characteristic for the discharge is the light emittance of the central region. Basically, low plasma radiation there means lower background signal, lower noise, and thus much better detection limit. Our numerical model is not designed to provide precise results for the plasma light emission, a much more detailed balance is needed for that. However, we can get a clue of the plasma radiation properties by looking at the excitation events which then could produce a photon at their deexcitation. Visible light can be emitted after the excitation of H_2 from electronic states, with term energies higher than 11 eV. Therefore, we assume that the number of emitted visible photons is correlated to the number of excited H_2 molecules (with term energies higher than 11 eV) and we can get an indirect indication of the plasma visible radiation by summing all the excitation collision rates for energies above 11 eV.

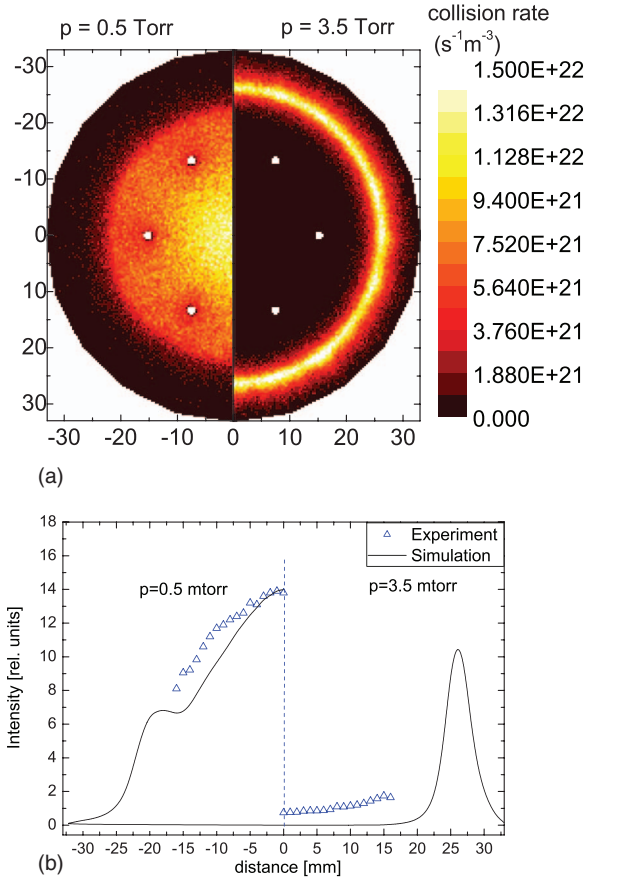

FIG. 9. (a) Excitation rate for energies above 11 eV. $p = 0.5$ Torr, $U = 590$ V and $p = 3.5$ Torr, $U = 292$ V. Both cases are for total current $I_t = 200$ mA. (b) Radial emission from the source in different pressure conditions. The dashed blue line indicates the center of the discharge.

Fig. 9(a) presents the distribution of the total excitation rate of H_2 molecules above 11 eV, i.e., $\sum_i \langle k_i n_e N_{H_2} \rangle_E$, where k_i is the rate coefficient of the ith process, n_e is the electron density, N_{H_2} is the H_2 density, and "$\langle\,\rangle_E$" means averaging over the electron energy distribution function (EEDF).

In order to compare the results from the numerical simulations, we decided to run an additional experiment which allows us to record the radiation along the axis for different radial positions in the discharge tube. For that purpose we constructed a collimation tube with an inner diameter of 1 mm and a length of 200 mm, which was installed parallel to the tube axes 10 mm from the window of the discharge tube. Only light emitted along the axis of the discharge for given radial position can be collected through this tube. It was done by an optical fibre (inner diameter of 0.5 mm) and a photomultiplier (FEU-17A). In this way we were able to record the axial emission of the discharge, changing the radial position of the collimation tube from the center of the discharge to the anode's rods. We were not able to measure light emission in the anode-cathode region due to obstruction from the end flanges. Fig. 9(b) shows the obtained experimental results (open triangles) compared with the averaged radial density of the excitation rates (solid line). The theoretical results for both pressures are rescaled in order to match the experimental value for $p = 0.5$ mTorr in the center of the tube.

TABLE I. Variation of the averaged electron energy in the discharge center as a function of the gas pressure.

I_t\p	3.5 Torr	1.3 Torr	0.5 Torr
100 mA	0.36 eV	1.42 eV	2.37 eV
200 mA	0.57 eV	2.67 eV	3.15 eV

In general, the numerical results for the excitation rates and the measured radiation have similar behaviour and relative variation for different values of the gas pressure. This is especially well seen for the low pressure case of 0.5 Torr. Both the theory and the experiment show that at this pressure the emission is concentrated mainly within the anode zone, in the center being about two times stronger than at the anodes. At 3.5 Torr the discharge has a dark central region and bright area in the anode-cathode region. According to the calculation the emission in the center of the discharge tube at 3.5 Torr is somewhat weaker than in reality, so the agreement is qualitative. The comparison here is rather difficult. On the one hand, the measurements are carried out up to the anode rods, i.e., only in the dark region. On the other hand, it is a well known disadvantage of the particle based models that they are not able to resolve quantities with large variation in magnitude across the discharge.

At low gas pressure and low density, the plasma is contained in the center with relatively high energy, resulting in highest excitation (Fig. 9(a), 0.5 Torr) and radiation (Fig. 9(b), 0.5 Torr) rates there. In contrast, at a higher pressure of 3.5 Torr, the center region is a low excitation region (Fig. 9(a), 3.5 Torr) compared to the anode-cathode space, which results in considerably lower light emission (Fig. 9(b), 3.5 Torr). The difference between the plasma emittance at high and low pressures is due to two reasons: At 3.5 Torr the electron density is slightly lower in the center (Table I) and the averaged electron energy in the central region is very low—around 0.57 eV. Table I shows the dependence of the averaged electron energy in the discharge center on the pressure obtained by the numerical model. A general behaviour typical for all types of discharges (Ref. 9) is a decrease of the electron temperature with the pressure increase. The averaged energy in the center of our discharge follows exactly the same trend and determines the light emission characteristics of the central region.

With respect to spectroscopy measurements, our target is to have lower light emission in the center which means lower averaged electron energy. According to Fig. 9 and Table I, this is achievable by pressure increase. In this cases, however, if the production of molecules is related to the sputtered material from the cathode (as it is in the case of NiH), the pressure increase reduces significantly the ion energy (see Fig. 5) at the cathode and thus the cathode sputtering could be reduced or even ceased. For efficient sputtering of different materials we need ion energy of at least 20–30 eV (Ref. 9). In such situations, the pressure increase might not be a straightforward solution. Instead, one needs to look for modification of other discharge parameters (like the discharge geometry and dimensions, for example) or to look for a compromise condition for the given application.

VI. CONCLUSIONS AND FUTURE PLANS

In this paper, a new construction of a discharge tube with coaxial geometry was investigated with respect to its applications in spectroscopic studies of metal hydrides. A prototype of the tube with eight separated Ni cathodes was tested. The total length of the cathodes is 250 mm. In pure hydrogen atmosphere, at pressures of about 200-300 mTorr, NiH densities of about $\sim 10^{12}$ cm^{-3} were produced. These relatively high densities and long absorption lengths make this source very attractive for absorption experiments since reliable signals (corresponding to 0.02% absorption) were detected even in a single pass configuration.

The present work has shown that the mechanisms for production of metal hydrides in different sources may be different. Contrary to the sources from Refs. 1 and 2 where highest molecular densities have been achieved in a Ar-H_2 mixture, in this source (similar to that from Ref. 3) signals were registered only in a pure hydrogen atmosphere.

At the working pressures of 200-800 mTorr, however, the emission in the central part of the tube is strong. The dark central zone is formed only at higher gas pressures (above 2 Torr), where the molecular density is below our detection threshold ($\sim 2 \times 10^{11}$ cm^{-3}). In order to study whether it is possible to optimize the discharge parameters and their geometry to achieve both goals simultaneously, we run a comprehensive simulation based on the PIC-MCC method. With few empirical parameters the model was able to describe quite well the experimentally measured emission in the central part of the tube. Analyzing the output of the simulations we correlated the emission in the tube with the energy distribution of the electrons in the plasma, whereas the production of molecules is most likely related to the energy distribution of the positive ions. Both parameters decrease in a similar manner with increase of the gas pressure; therefore, a precise and accurate balance is needed in order to propose a new tube geometry and discharge parameters with electron energy sufficiently low in the center of the tube and ion energy sufficiently high at the cathodes. Preliminary simulations have shown that at similar currents and pressures by increasing the cathodes' diameter without changing the anodes' diameter the emission in the center of the tube would be lower.

Even with the emitting plasma in its central zone, the current tube geometry can be a good source of metal hydrides for absorption measurements. The only drawback of the present construction is the lack of efficient cooling of the cathodes. In Fig. 10 we present a modified construction of the discharge tube where cooling of the cathodes is straightforward. The new tube is collected from aluminum rings, separated by rubber o-rings for sealing. The rings should be at least 10 mm thick in order to avoid galvanic contact between the rings after evacuating the tube. The cathodes, made of thin foil, are rolled on the inner side of the Al rings, thus ensuring good thermal contact. The high voltage is applied separately on each aluminum ring from outside the tube. The anode is formed by thin rods fixed in teflon rings, which are supported in the end flanges of the tube. The cathodes and the end flanges are pressed together by four long screws. The openings of the end flanges are designed to accept a standard KF50 flange, for

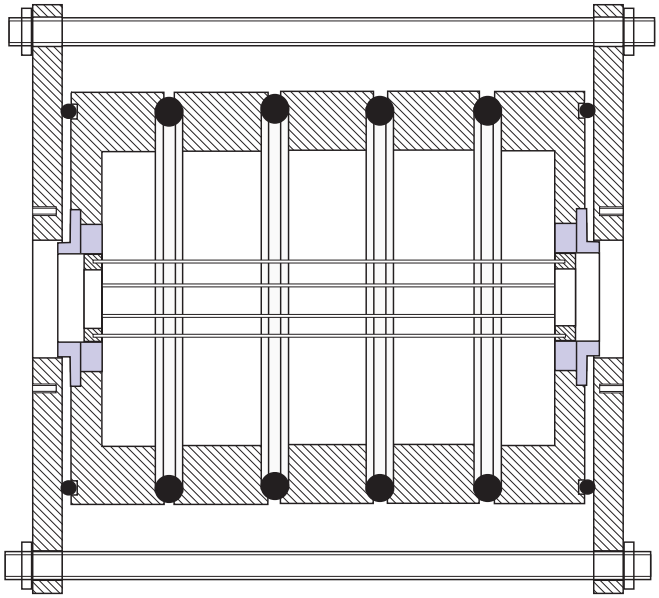

FIG. 10. Sketch of a metal version of the discharge tube. For sake of simplicity only three cathode rings are given.

installation of the tube windows and connections to the vacuum apparatus.

The advantage of this construction is that there is direct contact between the cathodes and the massive aluminum rings which can be cooled from outside passively by air or with air flow. It is easy to disassemble tube for replacement of the cathodes or to insert anode with a different outer diameter.

It is possible to think about the possible application of this discharge geometry for production of molecules other than hydrides by changing the gas (e.g., oxygen, nitrogen). In principle, the developed fluid and PIC/MCC methods can be used for preliminary estimation of the plasma parameters.

ACKNOWLEDGMENTS

A.P. and I.B. acknowledge the partial support from the Rila5/01/2011 exchange program and Sofia University Grant Nos. 143/2012 and 85/2013. Ts.P. and M.D. acknowledge the support from the European Community under the contract with Association EURATOM/INRNE.BG, the Bulgarian Science Fund through the Association EURATOM-INRNE, and International Atomic Energy Agency (IAEA) Research Contract No. 17125/R0 as a part of the IAEA CRP F13014 on "Utilisation of a Network of Small Magnetic Confinement Fusion Devices for Mainstream Fusion Research."

APPENDIX

The numerical model considers the following processes denoted in Tables II and III.

The spatial resolution used in the simulations was 200 × 100 cells. Only half of the domain is simulated due to symmetry. The time step was between 2×10^{-11} s and 5×10^{-11} s, depending on the conditions and mainly on the maximum electron velocity.

TABLE II. List of electron collision processes.

Process	Reference
$e + H \rightarrow e + H$ (elastic)	10 and 11
$e + H \rightarrow e + H^*$ (4 energy states)	12
$e + H \rightarrow 2e + H^+$ (ioniz.)	12
$e + H_2 \rightarrow e + H_2$ (elastic)	13
$e + H_2 \rightarrow 2e + H_2^+$ (ioniz.)	12
$e + H_2 \rightarrow 2e + H^+ + H$ (2 diss. ioniz.)	12
$e + H_2 \rightarrow 2e + H_2^*$ (17 electronic states)	12–16
$e + H_2^+ \rightarrow 2H$ (diss. recombination)	12
$e + H_2^+ \rightarrow e + H + H^+$ (diss. exc.)	12
$e + H_3^+ \rightarrow H_2^* + H^*$ or 3H (dissociation)	12
$e + H_3^+ \rightarrow e + H^+ + 2H$	12
$e + H_3^+ \rightarrow e + H^+ + H_2$	12
$e + H_3^+ \rightarrow e + H^+ + H_2$	12

TABLE III. List of heavy particles collision processes.

Process	Reference
$H^+ + H \rightarrow H + H^+$ (charge transfer)	17
$H^+ + H \rightarrow H^+ + H$ (elastic)	17
$H^+ + H_2 \rightarrow H^+ + H_2^*$ (2 rotational excit.)	18 and 19
$H^+ + H_2 \rightarrow H_2^+ + H$ (charge transfer)	18
$H^+ + H_2 \rightarrow H^+ + H_2$ (elastic)	18
$H_2^+ + H_2 \rightarrow H_2^+ + H_2$ (charge transfer)	18
$H_2^+ + H_2 \rightarrow H_3^+ + H$ (proton transfer)	19
$H_3^+ + H_2 \rightarrow H_3^+ + H_2$ (elastic)	18
$H_3^+ + H_2 \rightarrow H_2 + H_3^+$ (proton transfer)	18

[1] M. Li, J. A. Gray, and R. W. Field, "A multipass, magnetically, confined sputter source for absorption-based spectroscopy of transient molecules: the spectrum of NiH," Chem. Phys. **117**, 171–176 (1987).
[2] R. Vallon, S. H. Ashworth, P. Crozet, R. W. Field, D. Forthomme, H. Harker, C. Richard, and A. J. Ross, "Room-temperature metal-hydride discharge source, with observation on NiH and FeH," J. Phys. Chem. A **113**, 13159–13166 (2009).
[3] L. C. O'Brien and J. J. O'Brien, "Laboratory measurements of NiH by intracavity laser absorption spectroscopy," Astrophys. J. **621**, 554–556 (2005).
[4] Tsv. K. Popov, M. Dimitrova, and F. Dias, Vacuum **76**, 417–420 (2004).
[5] Tsv. K. Popov, M. Dimitrova, F. Dias, V. N. Tsaneva, N. A. Stelmashenko, M. G. Blamire, and Z. H. Barber, J. Phys.: Conf. Ser. **44**, 60–69 (2006).
[6] S. Shaji, J. Nunn, J. J. O'Brien, and L. C. O'Brien, "Intracavity laser absorption spectra of nickel hydride," Astrophys. J. **672**, 722–725 (2008).
[7] NIST:Atomic Spectra Database, see http://physics.nist.gov/PhysRefData/ASD/levels_form.html.
[8] K. Birdsall and A. B. Langdon, *Plasma Physics via Computer Simulation* (McGraw-Hill, New York, 1985).
[9] M. A. Lieberman and A. J. Lichtenberg, *Principles of Plasma Discharges and Materials Processing* (Wiley, New York, 1994).
[10] Y. Itikawa, "Momentum-transfer cross sections for electron collisions with atoms and molecules," At. Data Nucl. Data Tables **14**, 1–10 (1974).
[11] S. Trajmar and I. Kanik, "Atomic and molecular processes in fusion edge plasmas," in *Atomic and Molecular Processes in Fusion Edge Plasmas*, edited by R. K. Janev (Plenum, New York, 1995), p. 40.
[12] R. K. Janev, D. Reiter, and U. Samm, Collision processes in low-temperature hydrogen plasmas, see http://www.eirene.de/report_4105.pdf.
[13] S. J. Buckman and A. V. Phelps, "Vibrational excitation of D_2 by low energy electrons," J. Chem. Phys. **82**, 4999–5011 (1985).

[14]J. Yoon, M. Song, J. Han, S. Hwang, W. Chang, B. Lee, and Y. Itikawa, "Cross sections for electron collisions with hydrogen molecules," J. Phys. Chem. Ref. Data **37**, 913–931 (2008).
[15]H. Ehrhardt, L. Langhans, F. Linder, and H. S. Taylor, "Resonance scattering of slow electron from H_2 and CO angular distribution," Phys. Rev. **173**, 222–230 (1968).
[16]S. J. Buckman and A. V. Phelps, University of Colorado, JILA Information Center Report No. 27, see http://jilawww.colorado.edu/~avp/collision_data/electronneutral.
[17]P. S. Krstić and D. R. Schultz, "Elastic and related transport cross sections for collisions among isotopomers of $H^+ + H$, $H^+ + H_2$, $H^+ + He$, $H + H$, and $H + H_2$," *Atomic and Plasma-Material Interaction Data for Fusion* (International Atomic Energy Agency, Vienna, 1998), Vol. 8.
[18]A. V. Phelps, private communication (2007).
[19]S. J. Buckman and A. V. Phelps, "Cross sections and swarm coefficients for H^+, H_2^+, H_3^+, H, H_2, and H^- in H_2 for energies from 0.1 eV to 10 keV," J. Phys. Chem. Ref. Data **19**, 653–675 (1990).